Accepted Manuscript

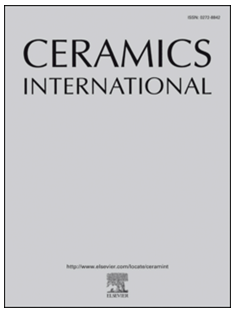

Non-destructive screening methodology based on ED-XRF for the classification of medieval and post-medieval archaeological ceramics

E. Calparsoro, Maite Maguregui, Hector Morillas, Gorka Arana, J.G. Iñañez

PII: S0272-8842(19)30439-0

DOI: https://doi.org/10.1016/j.ceramint.2019.02.138

Reference: CERI 20861

To appear in: *Ceramics International*

Received Date: 31 October 2018

Revised Date: 7 February 2019

Accepted Date: 20 February 2019

Please cite this article as: E. Calparsoro, M. Maguregui, H. Morillas, G. Arana, J.G. Iñañez, Non-destructive screening methodology based on ED-XRF for the classification of medieval and post-medieval archaeological ceramics, *Ceramics International* (2019), doi: https://doi.org/10.1016/j.ceramint.2019.02.138.

Non-destructive Screening Methodology based on ED-XRF for the classification of Medieval and post-Medieval Archaeological Ceramics

E. Calparsoro[a,*], Maite Maguregui[b], Hector Morillas[c], Gorka Arana[d], J.G. Iñañez[a]

[a] *GPAC, Built Heritage Research Group, University of the Basque Country UPV/EHU, Micaela Portilla Research Center, Justo Velez de Elorriaga 1, Vitoria-Gasteiz, Spain*
[b] *Department of Analytical Chemistry, Faculty of Pharmacy, University of the Basque Country UPV/EHU*
[c] *Department of Mathematics and Experimental Sciences Didactics, Faculty of Education, Philosophy and Anthropology,*
[d] *Department of Analytical Chemistry, University of the Basque Country UPV/EHU, Barrio Sarriena s/n Leioa, Spain*

Abstract

Compositional analysis of ceramics plays a crucial role in Archaeology because following the proper methodology, it enables to obtain knowledge about past human behavior. In this regard, X-Ray Fluorescence Spectrometry (XRF) involves promising possibilities on the non-destructive analysis of pottery. Nonetheless, in comparison to traditionally employed techniques such as ICP-MS or NAA, there are several limitations to overcome (e.g. limits of detection, precision, accuracy, etc.). The goal of this work was to develop a non-destructive multi-point strategy based on ED-XRF and, subsequently, assess to what extent a destructively obtained classification by ICP-MS can be reproduced by the one obtained non-destructively. The experiment was applied to a set of 47 representative Medieval and post-Medieval ceramics from the Iberian Peninsula corresponding to 4 archaeological sites. The results from both methods were explored statistically (HCA and PCA) and showed that the classification obtained non-destructively achieved a high-level of correspondence with the one obtained by ICP-MS. Thus, the screening potential of the methodology was demonstrated. Likewise, factors involved in the geochemical characterization such as instrumental parameters, concentration ranges of these ceramics typologies, their heterogeneity and the role of the ubiquitous lead glazes were addressed.

Keywords: `non-destructive analysis, screening, archaeological pottery, ED-XRF`

1. Introduction

Compositional analysis of ceramics is one of the most popular subjects in Archaeological Science [1, 2, 3]. The chemical fingerprint of the ceramics enables establishing the ceramic provenances and helps out building solid hypotheses regarding their historical implications and cultural trade-offs [4, 5, 6, 7]. A routine compositional analysis involves recognizing the different chemical patterns after applying an array of multivariate statistical strategies on the elemental compositional values [1, 5, 8]. In supervised learning, the ceramic sample can be ascribed to a certain source (e.g. a workshop) if it is accompanied by strong archaeological evidence (e.g. kiln, kiln utensils or potter mistakes). Afterward, the unknown ceramic sample can be collated with existing databases and either match existing referential units of compositional groups (URCG), or constitute new ones [5].

Ceramic analyses have been dominated by the use of destructive analytical techniques [9], such as neutron activation analysis (NAA), atomic absorption spectrometry (AAS), inductively coupled plasma atomic emission spectrometry (ICP-AES) and mass spectrometry (ICP-MS) [9, 10]. The most recent is ICP-MS, although this technique requires the total or partial destruction of the sample (ca. 250 mg are employed

*Corresponding author
Email address: `estefania.calparsoro@ehu.eus` (E. Calparsoro)

for ceramic analysis). Moreover, the sample manipulation and extraction techniques may influence the final results [11] and the problems of contaminations during the sample pre-treatment (e.g. acid digestion or alkaline fusion) and the interferences introduced by the addition of new compounds are still a challenge, even if attempts have been made to keep this analytical error to a minimum in similar matrices [12].

Alternatively, most of the current quantitative approaches for pottery characterization are based on X-ray fluorescence (XRF) [10, 13, 14, 15, 16], since with low sample preparation costs, it can provide simultaneous multi-elemental determinations for those elements with an atomic number higher than 10 in most of the cases (starting from Na)[9, 15].

Currently, there are three main XRF set-ups employed in pottery analysis: total reflection (TXRF), wavelength dispersive (WD-XRF) and energy dispersive (ED-XRF). The main advantage of TXRF over other XRF based techniques is the minimizing of matrix effects. Nonetheless, a sample preparation is still required, which usually implies the suspension of solid particles in a liquid carrier [17, 18, 19]. Application of this technique to pottery can be found in the literature [18, 20, 21, 22].

In contrast, ED-XRF and WD-XRF are more widely extended for archaeological pottery analysis (e.g. [23, 24]). Small sample masses are required (ca. 300 mg to some grams), pressed into homogeneous pellets or fused into beads, providing accurate determination of major (Na, Mg, Al, Si, K, Ca, Fe), minor (Ti, P, S, Mn), and trace (V, Ni, Cu, Zn, Br, Rb, Sr, Ba, Pb) elements [25, 26].

Benchtop ED-XRF is often preferred, despite WD-XRF offering better limits of detection (LOD), since using some set-ups, a previous sample preparation (e.g. powdering) is not required, although a minimum intervention to avoid surface contamination is always advisable. Although in self-made WD-XRF spectrometers measurements at low lateral resolutions (in the order of microns) can be achieved including polycapillary optics, frequently, commercial equipment do not allow a reduction of the X-ray beam diameter down to microns, and it is only possible to measure at millimeter scale. On the contrary, current commercial and conventional ED-XRF spectrometers allow acquiring measurements even down to 25 μm [27].

In addition, works using pXRF (portable XRF) are also on the increase [28, 29]. Nevertheless, frequently the calibrations implemented in the instruments are not modifiable and some devices do not allow data treatment in the implemented software, becoming mere black boxes, where the only option is to extract the spectra and treat them with an external software.[30].

Thus, they often fail to successfully represent the reality of the ceramic matrix. The latest versions of pXRF devices have improved the Limits of Detection (LOD) of the lightest elements (Na and Mg mainly) and in some cases, it is also possible to acquire measurements under vacuum or He atmosphere, improving to a greater extent the LODs of these elements. In the literature, the applicability of pXRF to ceramic analysis has been widely discussed [13, 15, 26, 31].

In this work, a non-destructive approach was developed by using a benchtop ED-XRF equipped with a dual automatically switchable collimation system, with lateral resolutions from 1 mm down to 25 μm. The proposed screening methodology aims to present a robust and reliable alternative offering several advantages over more traditional analytical methodologies, such as avoiding significantly the process of sample preparation and performing a non-destructive automatic analysis. To assess the discrimination capability of the non-destructive technique, firstly ICP-MS analyses were carried out and different compositional groups were identified.

Archaeological ceramic samples showing compositional discrepancies at different levels (in major and/or minor elements) and corresponding to several compositional groups were selected, in order to be able to evaluate resolution level of the non-destructively obtained classification. Furthermore, the specific issues affecting the types of ceramics from the Medieval and post-Medieval periods manufactured in the pottery workshops of the Iberian Peninsula, such as the presence of lead glazes, or their heterogeneity level, were addressed.

2. Materials and Methods

2.1. Ceramic sample

The sample consists on 47 archaeological ceramics unearthed from four different sites located in the northern Iberian Peninsula. These are the towns of Durango, Elosu and Orduña in The Basque Country

Source	Acronym	Description	Provider	N	References
Logroño	LOG	Hospital Viejo street (3 Medieval kilns)	ArqueoRioja	n= 12	[32]
Orduña	ORD	Basque traditional post-Medieval kiln	Bizkaiko Arkeologia Museoa	n= 10	[33, 34, 35]
Durango	DUR	Basque traditional post-Medieval kiln	Museo de Ollerias	n= 5	[35, 36]
Elosu	ELS	Basque traditional post-Medieval kiln	Museo de Ollerias	n=20	[35, 36]

Table 1: Brief description of the archaeological sites where ceramics have been obtained from.

(TBC) and the city of Logroño in La Rioja (LR) and date back to chronologies between the $13^{th}$to the 20^{th}centuries (see Table 1 and Figure 1).

Typologically, the ceramics comprise diverse pieces; including kiln-utensils such as trivets and tableware such as bowls, basins, vessels and jars. Their decoration varies from unglazed or translucent glazed pieces to basic decorated tin-lead-glazed in the latest chronologies. For more details see supplementary material.

2.2. Inductively Coupled Plasma Mass Spectrometry (ICP-MS)

For the ICP-MS analysis, ca. 10-15 g of each sample was powdered in a planetary mill using tungsten carbide cells for 2-4 min at 300 rpm. Prior to milling, glazes and outer surfaces were mechanically removed in order to minimize contamination from glaze and soil into the sample. Powdered specimens were stored in polyethylene vials for transportation to the laboratory. Powdered samples were calcined at 1000°C. Then, along with the Certified Reference Materials (CRM) from the Geological Survey Japan (JB-3, JA-2, JG-1A, JG-2) used for the calibration of ICP-MS, they were fused using a Fluxy automatic gas fluxer (Corporation Scientifique Claisse, Canada). These CRMs are based on igneous rocks and this method has been previously optimized for similar matrices (see elsewhere [12]).

The internal standards (Sc, Y, In, Be, Bi) and ICP-MS calibration standards solutions were prepared from 1000 $\mu g/mL$ stock solutions of Alfa Aesar (Specpure©, Plasma standard solution, Germany) inside a class 100 clean room. All solutions were prepared using Milli-Q quality water. Calibration standards and the samples' dilutions were prepared gravimetrically using an analytical balance model Mettler-Toledo XS205 (Colombus, OH, USA) with an uncertainty of ± 0.00001 g. The accuracy and reproducibility of the method were checked by repetitive non-analyses (n = 3) of the mentioned CRMs.

^{27}Al, ^{28}Si,^{31}P, ^{44}Ca, ^{85}Rb, ^{88}Sr, ^{90}Zr, ^{93}Nb, ^{120}Sn, ^{133}Cs, ^{137}Ba, ^{139}La, ^{140}Ce, ^{141}Pr, ^{142}Nd, ^{147}Sm, ^{153}Eu, ^{158}Gd,^{159}Tb, ^{164}Dy, ^{165}Ho, ^{166}Er,^{169}Tm, ^{174}Yb, ^{175}Lu, ^{180}Hf, ^{181}Ta, ^{232}Th, ^{208}Pb and ^{238}U isotopes were determined in standard mode and ^{23}Na, ^{24}Mg, ^{39}K, ^{47}Ti,^{51}V, ^{52}Cr, ^{55}Mn, ^{56}Fe, ^{59}Co, ^{60}Ni, ^{65}Cu and ^{66}Zn isotopes were determined in Kinetic Energy Discrimination (KED) mode with He in order to eliminate possible polyatomic interferences. The quantitative data were acquired and analyzed by using the Nexion 1.5 software (Perkin Elmer SCIEXTM, Ontario, Canada).

The LODs were calculated after the following formula:

$$Y_{LOD} = \overline{Y}_{bl} + 3S_{bl} \tag{1}$$

where $\overline{Y}_{bl}$ is the average signal of three blank analyses and S_{bl} is the standard deviation of them. Once the Y_{LOD} values were obtained, and using the calibration curve of each specific element, the concentration associated with the LOD was extracted.

2.3. Energy Dispersive X-Ray Fluorescence Spectrometry (ED-XRF)

For the compositional characterization of the ceramic pastes and CRMs, the M4 TORNADO (Bruker Nano GmbH, Berlin, Germany) ED-XRF spectrometer was used. The analyses were performed directly on the section of the sample cut by a precision cutter and placed directly in the instrument chamber. Although the instrument allows introducing samples up to 33 x 17 cm and 5 kg, it was decided to cut the samples to obtain a flat surface for analysis, to prevent analyzing areas with external contaminations and to have access to the original bulk of the sample. The set-up of this instrument allows measuring at two lateral

resolutions, 1 mm using the mechanical collimator and down to 25 μm by means of the polycapillary optics implemented in the instrument.

The X-ray tube incorporated is a micro-focus side window Rh tube powered by a low-power HV generator and cooled by air. The X-ray tube can work at a maximum voltage of 50 kV and at a maximum current of 700 μA for 1 mm collimation and up to 600 μA working down to 25μm lateral resolution. The detection of the fluorescence radiation is performed by an XFlash® silicon drift detector with a 30 mm^2 sensitive area and energy resolution of 145 eV for Mn-K_α. In order to improve the detection of the lightest elements (Z<11), filters were not used and measurements were acquired under vacuum (20 mbar). To achieve the vacuum, a diaphragm pump MV 10 N VARIO-B was used. For the focusing of the area under study, two video-microscopes were used, one of them to explore the sample under a low magnification (1 cm^2 area), and the other one to perform the final focusing (1 mm^2 area). The spectral data acquisition and treatment was performed using the M4 software from Bruker. For further details on the measurement conditions (e.g. times, collimator selection and number of analyses) see section 4. Interferences introduced by matrix effects based on the acquired spectra and pile up corrections are corrected by the software. The software also allows the matrix composition to be inserted externally.

The Hyper Maps presented in this work were obtained using the polycapillary optics (down to 25μm of lateral resolution). Prior to obtaining the Hyper Maps, an elemental assignation and deconvolution of the spectral information was conducted. The elemental maps were obtained according to the intensity of the K_α line of each element detected in the present work. For those elements included in the CRM SRM679, the LODs were calculated according to the measurements carried out as pressed pellets following this formula:

$$LOD = 3C\sqrt{\frac{Background}{NetIntensity}} \tag{2}$$

where C is the real concentration and the background intensity was obtained from the spectra. In this formula, the net intensity was obtained subtracting the background (counts) from the element peak intensity (counts). The LODs of those elements not included in the certification were approximated according to the theoretical values provided by Bruker.

2.4. Data treatment

The statistical analysis applied in the current work is based on Aitchison's approach and Buxeda's observations on compositional data [23, 37, 38].

First of all, in order to compensate for the differences between absolute scales of major and trace elements, a logarithmic transformation was applied, this choice being the most used in the literature [39, 40, 41, 42]. Thus, any underestimation of the contribution of trace elements (that can play a crucial role when differentiating certain compositional groups) is avoided [1].

The comparisons were performed as discussed by Aitchison [43] by using the ratios of logarithms obtained by dividing all the chemical components by a selected component, overcoming in this way the compositional data problem called *close to unit sum*, which occurs when data necessarily must add up to 100% and which induces the variables to be codependent [38].

The selection of the component used as divisor depends on the statistical analysis to be performed. For the principal component analysis (PCA), the component that introduces the lowest chemical variability to the entire set of specimens is taken into consideration. This is called the additive log ratio transformation (alr). Whereas, for the hierarchical clustering analysis (HCA), the geometric mean was used as the divisor (i.e. centered log ratio (clr) transformation). For the HCA, the squared Euclidean distance is graphically represented using the centroid agglomerative algorithm. These transformations were applied to both concentrations obtained by ICP-MS and net intensities acquired by ED-XRF.

The software employed for all the transformations, statistical analysis and data visualization was R, an open source environment for statistical analysis. Packages like "compositions" developed by Van de Boogart [44] and its routines developed by J. Buxeda i Garrigòs were employed as well as ad hoc work flows performed for this specific project following the model that can be consulted in the repository published on the GitHub website [45].

3. ICP-MS Results

Variable	ELS	SD	DUR	SD	ORD	SD	LOG	SD	LOG033	LOG038
Al_2O_3	18	1	17	1	15	2	20	3	16	13
CaO	13	4	15	2	19	2	9	1	13	24
Fe_2O_3	4.8	0.2	4.9	0.2	4.1	0.4	7.5	0.3	5.3	4.7
K_2O	2.6	0.2	2.1	0.2	1.9	0.3	3.2	0.1	2.8	2.4
MgO	0.67	0.08	1.72	0.05	1.20	0.30	2.10	0.20	1.77	2.53
MnO	0.024	0.009	0.100	0.040	0.032	0.007	0.038	0.004	0.042	0.057
Na_2O	0.81	0.08	0.67	0.06	1.50	0.30	0.70	0.06	0.65	0.36
P_2O_5	0.18	0.20	0.14	0.01	0.70	0.91	0.46	0.24	0.28	0.39
SiO_2	60	5	64	3	51	10	43	2	38	40
TiO_2	0.75	0.12	0.72	0.01	0.63	0.10	0.81	0.03	0.63	0.67
Ba	452	34	436	49	300	53	586	57	517	487
Ce	89	6	79	3	68	9	117	4	91	80
Co	49	20	95	23	18	7	23	6	16	18
Cr	100	14	85	6	98	9	96	19	65	62
Cs	15	2	13	1	11	3	20	3	18	6
Cu	47	49	54	41	45	22	36	35	28	161
Dy	4.8	0.5	4.4	0.3	3.9	0.6	5.7	0.2	5.2	5.2
Er	2.6	0.2	2.3	0.1	2.3	0.4	2.9	0.1	2.8	2.7
Eu	1.2	0.2	1.2	0.1	0.9	0.2	1.8	0.1	1.4	1.4
Gd	5.8	0.6	5.7	0.1	4.5	0.8	9.1	0.4	7.4	7.2
Hf	6.9	0.7	6.1	0.2	6.4	1.7	2.8	0.2	3.4	3.6
Ho	0.76	0.08	0.67	0.03	0.74	0.10	1.00	0.04	0.92	0.94
La	44	3	41	1	32	4	57	2	44	41
Lu	0.46	0.05	0.40	0.03	0.34	0.06	0.43	0.01	0.42	0.39
Nb	21	2	23	1	17	3	20	1	18	16
Nd	40	4	35	1	28	4	47	1	38	35
Ni	20	3	<LOD		20	4	68	17	63	49
Pb	(204 - 12x10^3)		(377 - 5.5x10^3)		(339 - 10.1x10^3)		(37 - 2.65x10^3)		1.73 x10^3	2.58 x10^3
Pr	11.0	0.7	9.1	0.3	7.5	1.0	12.0	0.4	9.6	8.8
Rb	186	12	189	17	122	32	149	7	132	80
Sm	7.3	0.8	6.3	0.2	5.1	0.8	9.4	0.3	7.7	7.0
Sn	(165 - 377)		62	30	35	24	5	1	49	22
Sr	473	97	329	18	523	108	494	57	677	644
Ta	2.5	0.3	2.5	0.08	2.5	0.4	1.2	0.1	1.1	1.0
Tb	0.87	0.10	0.78	0.04	0.67	0.12	1.01	0.04	0.89	0.86
Th	20	1	14	1	13	1	11	1	8	8
Tm	0.44	0.05	0.40	0.02	0.33	0.06	0.51	0.02	0.47	0.50
U	3.9	0.4	3.3	0.2	3.3	0.6	3.0	0.1	2.9	2.5
V	89	18	81	7	65	9	139	7	83	74
Yb	2.6	0.3	2.3	0.1	2.4	0.4	3.0	0.2	2.9	2.8
Zn	<LOD	<LOD	100	51	94	14	94	14	93	83
Zr	237	26	219	11	250	67	191	15	222	252

Table 2: Mean concentrations and standard deviation (SD) values of each compositional group, obtained by ICP-MS and expressed in μg/g (oxides are expressed in wt%). <LOD: under limit of detection. For Pb concentration ranges are expressed due to the high RSD.

Through ICP-MS, the quantification of 42 elements was obtained. In Figure 2 the plot of the compo-

sitional variation matrix is shown. The graph displays the individual contribution of the variability from each element to the whole dataset, from the highest to the lowest[38]. The most varying element of the dataset containing 47 specimens is Pb, followed by Sn, while the element showing least variation is Lu. The total variation (ν_τ) describes the evenness of the ceramic set in terms of composition, and according to this metric, the polygenic or monogenic nature of the compositional data is defined [38].

3.1. Sources of variability

The total variation (ν_τ) for the analyzed samples is 7.69 (see Figure 2), depicting an overall strong variability among the dataset. This is normally the sign of a clear polygenic nature of the dataset (i.e. several chemical groups are present) [38]. However, for proper statistical analysis, some assumptions regarding the origin of the variability must be considered. Consequently, not all quantified elements will be employed for the chemometric analysis.

Archaeological ceramics can undergo alteration or contamination processes that affect the observed final composition. On the one hand, Pb and Sn are elements that are ubiquitous in tin-lead glazes, and might diffuse from the glaze into the clay body during the firing process [46]. Indeed, in our specific case, these two elements present the highest variability (see Figure 2).

Beyond the high variability, it must be highlighted that the ceramics of the regions under study present an overall high concentration of Pb, and the composition varies from tens up to ca. 10^3 μg/g with a normal distribution among the studied samples. The contribution of the lead glazes is depicted by the lower Pb concentration of unglazed ceramics (e.g. LOG006, LOG019, LOG003, LOG002), whereas the glazed ones show an enrichment of Pb (LOG0072, LOG074 and to a lesser extent LOG075). However, this is not the rule. The two highest concentration of Pb are shown by the unglazed trivet ORD065, that shows 10.1x10^3 μg/g and the tin-lead glazed ELS038, showing a striking concentration of 12.9x10^3 μg/g. For more details see supplementary material.

Moreover, due to post-depositional contaminations from P_2O_5 occurring in the soil waters, the concentration of this compound might vary depending on the exact burial location of the ceramics[47]. Thus, its variability is not connected to the clay type but to alterations that result in random concentrations of P, which indeed, is the third most varying element in our dataset (see Figure 2).

Likewise, the next most varying element, Cu, showed a high variability that responds to several outlier values in the samples of each site. The source of this variability is usually the post-depositional contamination [23], and regarding the unequally distributed variability of Cu, it was decided not to consider it for the statistical analysis.

In addition, the sample preparation process can be another source of variability. The use of a tungsten carbide cell for milling the samples can alter Co and Ta concentrations since these are present in the cell alloy and can be transferred to the sample when milling [11].

Finally, some values of Zn and Ni were below or very close to the limit of detection (LOD). Thus, these elements were not considered in the statistical treatment.

Furthermore, the concentrations of Rb, Na_2O and K_2O were omitted from the statistical analysis due to the possible presence of a double process of alteration of the vitreous phase of the ceramic paste with leaching of K_2O and Rb, and the subsequent crystallization of analcime, a sodium zeolite with the fixation of Na_2O from the water circulating in the soil [48, 49]. In this way, the contribution of this double process of alteration and contamination is difficult to quantify. Preliminary analyses performed by X-ray diffraction did not reveal the presence of analcime in these samples. Nevertheless, it was decided to omit these elements to reduce the possibility of adding variations stemming from post-depositional sources.

Finally, influence of the technological choices on the concentrations of CaO and Sr was considered (in nature, the presence of Ca is usually accompanied by Sr). In Archaeology, ceramics are often referred to as

calcareous or non-calcareous, according to their reddish or buffer color appearance, which mainly depends on the CaO concentration, among other factors (firing atmosphere, temperature, clay composition, etc.). Thus, the concentrations of CaO and Sr are relevant as they can determine the final appearance. Nevertheless, they can never be the main markers for provenance studies as they could give spurious classifications. The increment of the concentration of CaO and Sr could be due to the use of clay mixtures, including more calcareous pastes, or to the addition of calcite grains like tempers to the ceramic paste [50]. Depending on the nature of the calcite present in the potsherd (primary, secondary, reformed, precipitated, etc.) it can affect the paste's chemical composition [50, 23, 49] and also the trace elements associated with the calcite could be another source of variability. For instance, in the case of Elosu, ethnographic works reported the mixing in the respective proportion 25/75 of two types of clays extracted nearby the ceramic kiln: the so-called "white" (high calcareous) and "red" clays [35, p. 16]. In the present work, ICP-MS results showed that the classification remains equal, regardless of the use of these elements in the statistics as discussed later, guaranteeing that the clusters are not biased by the concentration of these elements.

3.2. Clustering by ICP-MS

The resulting dendrogram after the HCA (see Figure 3) depicts a clear divergence between the groupings of La Rioja (LR) and The Basque Country (TBC), as well as two individual cases that will be discussed later (LOG038 and LOG033). The characterizing concentrations of each group are shown in Table 2. The LR grouping shows an overall enrichment on minor and trace elements, as well as on Fe_2O_3 (7.5 wt% vs 4.0-5.4 wt% range among all groups) . In contrast, the Basque grouping (TBC) shows an overall higher concentration of trace elements such as Th, Zr and Hf, pointing to different sources (see Figure 3 and Table 2) The TBC group, which is also highlighted by pastes richer in CaO, is further split into three groups according to their corresponding provenances: ORD (Orduña), ELS (Elosu) and DUR (Durango).

The HCA and PCA point out that within the TBC groups, DUR displays marked chemical differences in MnO and MgO. On the one hand, the DUR group shows an overall higher presence of MnO (0.10 wt%) that at least doubles the remaining concentrations of the whole dataset (0.025-0.040 wt%). On the other hand, it shows the highest MgO concentration (1.7 wt%) among TBC groups (0.67-1.2 wt%), being the key element to discern it from the DUR group. As a consequence, the crucial role of MgO distinguishing the DUR group within the TBC grouping is highlighted. Moreover, the difference of ORD is given by its lower concentration of Al_2O_3 (15 wt%), higher CaO (19 wt%) and also Na_2O (1.5 wt%) along with an overall lower concentration of trace elements. In contrast, ELS shows an increment of minor and trace elements such as Cr, Lu, Sm, Tb, Tm, U, V and Yb, and especially Th, showing a concentration of 20.5 μg/g over a range of 12.5-14.5 μg/g among the TBC groups (see Table 2).

In addition, two samples unearthed in Logroño and showing notable compositional differences were identified: LOG033 and LOG038. Both HCA and PCA indicate the separated nature of these individuals. While the former (LOG033) falls into the clade of LR grouping in HCA, a general different concentration in minor and trace elements and, remarkably, a lower concentration of MgO (1.8 wt% over the range of the LR samples 2.1-2.5 wt%) is responsible for its detachment from that group.

The latter (LOG038) differs from all the remaining sherds due to numerous minor and trace elements (see Table 2). It is also the most calcareous sherd of the whole ceramic ensemble (23.8 wt% CaO). Previous technological characterizations and provenance studies by NAA [36, 51] suggested its Valencian provenance, which includes the decorative blue motifs on tin-lead glaze coating that are characteristic of the very well known Iberian production of Paterna [52].

4. ED-XRF Results

4.1. Measurement parameters

From the options that can be set in the instrument, first of all, three different variables were optimized: (i) measurement time, (ii) voltage and (iii) current applied to the Rh tube. To determine the measurement time at which it is not possible to improve the signal to noise ratio (SNR) and therefore, the limit of

detection, measurements at different times (100 s, 150 s, 200 s, 250 s and 300 s) were conducted on different ceramics (one from each group). Considering that the dead time was the same in all the ceramics ($\approx 1\%$), real-time was selected in all the measurements.

The SNRs for trace elements (μg/g level) in each sample were calculated, obtaining values much higher than three at 200 s. The American Chemical Society recommends that to certify that a spectral peak can be associated with the presence of a specific element/compound, its SNR must be three or greater [53]. In our specific measurements and in some cases for some specific elements, the SNR was lower than three at 100 or 150 s, thus it was decided to establish 200 s as the best measuring time. This measuring time allowed us to acquire representative values of each sample (50 points measured) in less than 3 hours per sample.

The X-ray tube can work at a maximum voltage of 50 KV and at a maximum current of 700 μA, which were found to be the optimal conditions for the spectra acquisition at 1 mm lateral resolution. At lower voltages and current, the net counts registered decreased and the spectral background was not improved.

Regarding the computing possibilities of the commercial software used for the spectra interpretation, this includes several semiquantitative approaches based on fundamental parameters (FP). On trials applied to CRMs (SRM679), from these pre-configured "Oxides method" and "Spectrum elements" methods, the former showed better results since it assumes the elements are present in their oxide form, approaching better the reality of the archaeological samples that mainly include clay minerals (e.g. Silicon oxides and iron oxides) . However, considering that both FP-methods are not created for a specific kind of matrix such as ceramic, the quantitative values obtained using either of these methods showed high deviations from real values, over the analytically acceptable thresholds. Therefore, assuming that we can only work in terms of a semiquantitative approach, instead of concentrations, net counts were used to construct the ED-XRF-based classification model. Indeed, when the purpose is to obtain a classification based on relative values and not absolute ones, the use of net counts is recommended since in analyses performed under the same conditions net counts provide the most reliable values. In contrast, quantitative results are mostly necessary only to compare results acquired at different laboratories.

Nevertheless, it must be regarded that for a given concentration, in ED-XRF the peak intensities will be significantly lower for light elements than for heavier elements, since the ionization cross section is much lower for light elements, and the low energy X-rays are easily absorbed by any material in their path. This could especially affect the discrimination of samples that rely on the difference in light elements, such as Al or Si. Therefore, in light of these limitations, the screening nature of the current methodology is depicted.

4.2. Lateral Resolution

The energy flux at the sample, which is mainly governed by the optics selected, will be higher using the polycapillary optics instead of the mechanical collimation (down to 25 μm vs 1 mm lateral resolution respectively). Thus, at down to 25 μm the detection of the lighter elements in the sample would be improved. Therefore, it could be reasonable to select this lateral resolution to construct the ED-XRF model. However, the particle size of the CRM used in this work is higher than 75 μm. Thus, it is expected that the CRM prepared as pressed pellet or Mylar films will be non-homogeneous at down to 25 μm; indeed, considering that the CRM has been ball milled and passed through a mesh sieve, it is expected that the ceramic bulk of real samples will be more heterogeneous at this lower lateral resolution. This observation will be confirmed in the following sections. In Table 3 the % Relative Standard Deviation (%RSD) values for the CRM prepared as pressed pellet and in Mylar films are presented.

Not surprisingly, for all the elements the collimator of 1 mm provided lower RSDs. Indeed, most of the values were half of those obtained at 25 μm, providing RSDs of ca. 15-20%, with the exception of Cl, As and Pb. The high %RSD values of Pb (83%) suggested that the distribution of this element was very heterogeneous among the pellet. Additionally, the high %RSD value achieved for Cl could be related to the high LOD for this element using the current set up with an Rh X-ray tube . The lower % RSD values obtained at 1 mm in the mylar sandwich suggested that the CRM was not homogeneously prepared as pressed pellet at down to 25 μm. Considering these results, to construct the non-destructive model by ED-XRF, ceramic samples were measured at 1 mm lateral resolution. A comparison of the areas covered by each spot can be observed in Figure 4, and the most common inclusion sizes are within the spot of 1 mm.

Element RSD (%)	25 μm	1 mm
Al	8	2 (2)
Si	9	1 (1)
Cl	26	50 (45)
K	13	1 (1)
Ca	54	6 (4)
Ti	9	2 (1)
V	16	7 (7)
Cr	14	16 (11)
Mn	16	5 (5)
Fe	22	2 (1)
Ni	34	19 (10)
Cu	37	16 (16)
Zn	38	7 (4)
Ga	42	13 (13)
As	80	28 (15)
Rb	47	4 (2)
Sr	51	8 (4)
Y	39	12 (9)
Zr	40	5 (4)
Pb	183	83 (75)

Table 3: %RSD values obtained measuring by ED-XRF the brick clay (SRM679) CRM pressed in Mylar films and using the net counts extracted at 1 mm vs 25 μm of lateral resolutions. The values for CRM prepared as pressed pellet form are included in parenthesis

4.3. Representativeness of the sample

It was decided to acquire 50 replicate analyses per sample since for the morphology of the potsherds under study (pieces of ca. 4 cm on the longest side) this amount was considered to cover sufficiently each surface under analysis (the section of the sample cut by a precision cutter), thus being representative of the geochemistry of each sample. Nevertheless, the number of analyses can be easily adapted to the requirements of each ceramic set. In addition, another interesting capability implemented in the ED-XRF software is that it allows selecting manually or automatically (with different grid modes, random and uniform) the exact locations of measurement. Therefore, the analyst can determine which spot to select, something that is especially useful in ceramics presenting challenging surfaces (e.g. with big inclusions, glazed, etc.). In the current ceramic set, as most of the ceramics were glazed, the selection of the measurement point was made manually, allowing it to be easily adapted to the random shapes of the ceramics. In cases where the sample surface can be rectangular or square, the automatic point selection could be more adequate, but in the case of archaeological ceramics, the automatic selection may leave out relevant parts of the potsherd . It was evident that if the selection was performed close to the glaze, concentrations for Pb increased considerably, as a result of the diffusion of Pb from the glaze into the clay body [46].

In addition, the ED-XRF software implements the auto-focus option that along with the programmability allows the system to switch from one sample to another automatically. Indeed, this is one of the most advantageous features, since it permits programming all the analyses in advance.

4.4. Dynamic ranges, LODs, and LOQs

4.4.1. Elements $Z < 20$

Generally speaking the LOD of the ED-XRF improves with the increase of the atomic number (Z). Although this property is not linear, the elements below Na (Z=11) will not be detectable [26, 54]. The

concentration ranges of Na_2O in the analyzed ceramics are between 0.7 and 1.5 Wt% (as seen by the ICP-MS results). Therefore, the Na present in the archaeological ceramics is virtually invisible for the detector by ED-XRF with a Rh excitation (another type of excitation, such as W, could be more suitable for the evaluation of the lighter elements).

Likewise, the differentiation of Mg, P and S contribution from the background is hindered due to two reasons: (i) their low concentration in archaeological ceramics and (ii) the low energy of the resulting emitted fluorescence, which can easily be reabsorbed by the matrix [13], the detector window, contact and Si dead-layer. The detections are even worse if the mechanical collimation is used, as mentioned before . Moreover, in the case of P the scape peak of Ca can be problematic if a proper deconvolution is not carried out, overestimating its contribution.

Nevertheless, S and P could be disregarded to a certain extent due to their variability, which can be strongly dependent on external factors and not characteristic from the ceramic pastes. In contrast, Mg, which is also difficult to properly detect, might play a role characterizing compositional groups, as is the case of the DUR group, which can be differentiated from its compositional neighbor ELS due to Mg (apart from Mn), as shown by the ICP-MS results. LOG033 sample is also differentiated from the LOG group by a lower Mg concentration (see Table 2).

Thus, from the low or mid Z elements that are of interest in the archaeological ceramics (Na, Mg, Al, Si, P, S, K and Ca) [26], only Al, Si, K and Ca have shown high enough concentrations for their detection by ED-XRF with the current set-up.

4.4.2. Elements $Z > 20$

In ED-XRF, the LODs are significantly better especially, for elements Z>15. The estimated LODs for the ED-XRF instrument used in this work are (in μg/g), 100 for Ti, 80 for Cr, 50 for Mn, 40 for Fe, 30 for Ni, 20 for Cu and Zn, and 300 and 200 for Sn and Pb respectively.

Therefore, according to the ICP-MS results, elements such as Ti, Mn, Fe and Pb, are in concentrations rich enough to provide consistent semiquantitative values in these conditions. In contrast, the values of Sn are below 200 μg/g for all the samples as seen by ICP-MS. In rich Fe samples, the contribution of the escape peak from Fe (4.660 keV) has to be carefully addressed since it overlaps the K_α line of Ti (4.508 keV).

Likewise, the spectral lines of Ti, V, Cr, Mn, Fe and Co, should be carefully selected for a proper deconvolution since the K_α lines of these elements might overlap the K_β lines of the element bearing the previous atomic number. Although the concentrations of V, Cr, Mn and Co are much lower than those of Ti and Fe in the samples, its minimum contribution to the Ti and Fe signals should be avoided through a proper deconvolution of the signals. The concentrations of V, Cr, Co, Ni, Cu and Zn in the ceramic set fall over the detection limits, although in the best cases the obtained values are under the limit of quantification (LOQ).

For Sr, the average concentration of each group ranges from 329 to 677 μg/g. Therefore, it should be perfectly detectable by ED-XRF. However, its presence is normally associated with Ca, and thus might respond to technological choices rather than to the geochemical fingerprint of the ceramic as has been discussed before. Consequently, its relevance in the statistical analysis should be carefully addressed.

The estimated LOD of Rb should be ca. 30 μg/g, which is easily exceeded by concentrations present in the ceramics (80 -189 μg/g). In the case Rb, Ga and Y, apart from showing very low net counts, the influence of the presence of Pb should be highlighted, as is addressed later.

In summary, according to the concentrations of the archaeological ceramics with the current set-up, only the following elements were considered for further evaluation: Ti, Mn, Fe and Zr, whereas Sr could be used with certain restrictions.

4.5. Heterogeneity on Archaeological Ceramics

It is mandatory to understand the condition of archaeological ceramics of synthetic and heterogeneous materials since they present a special set of challenges for analysis using XRF non-destructively. Thus, beyond the factors mentioned so far (escape peaks, LODs, attenuations, etc.), other sources of variability specifically linked to the ceramics matrices may hinder a proper geochemical characterization, with the most

relevant being: the sample heterogeneity, grain size and mineralogical effects [13, 31, 55]. The interactions of the X-rays can be strongly affected, but not only, by the heterogeneous mixture of the phases. Moreover, the grain size will influence the penetration depth of the beam. Finer grains will allow a deeper penetration, whereas bigger ones may interact alone with the beam, limiting the mass of the analyzed composition. Moreover, the crystal structure, density and composition of the corresponding grains will also affect the interaction with the X-rays [13]. Archaeological ceramics include clays that are made from minerals of different grain sizes and these are not milled when analyzed by ED-XRF in a non-destructive manner. Therefore, their heterogeneity is one of the most common discussed challenges.

In order to evaluate the heterogeneity of real archaeological samples, the resulting RSDs from the net count values corresponding to 50 analysis points per each sample were considered (see Figures 5). The plot enables assessing the dispersion of the data in terms of RSD for each element, which varies from less than 5% in the best cases (Al or Si) to more than 100% (Ga), with exception of Pb (that passes 200%). Generally speaking, the more heterogeneous the samples the higher the RSD values. However, some elements have been included whose high RSD might be due to the difficulty of the detector to register the low quantity of net counts.

According to Figure 5, two trends were observed: elements having predominantly RSDs between %1-25 (Al, Si, K, Ca, Ti, Fe, Rb, Sr, Zr) and those with higher RSDs, up to 80% (V, Cr, Mn, Co, Zn, Ga, and Y). From the latter elements, only Mn presents a valid concentration range for the ED-XRF analysis. However, according to the high RSD, the heterogeneity of this element is too high to be considered for the statistical analysis. Note that some of these elements were disregarded due to low signals (Cr, V, Co, Ga, and Y) or influence by Pb (Ga, Rb and Y). However, their RSD might still provide hints on their distribution.

According to these results, the best RSD values are provided by Al, Si and Fe. Moreover, in the plot (see Figure 5) it can be observed how the heterogeneity varies from one compositional group to another, regardless of the potsherds quantity. For instance, DUR (n=5), showed frequently higher variability than ORD (n=10), which served to shed light on the heterogeneity of each compositional group. Therefore, it is clear that the variability in RSD does not rely on the number of samples, but rather on the compositional distribution of each group.

Moreover, in order to evaluate the distribution of each element, the current set-up allows subjecting the samples to imaging analysis at down to 25 μm of lateral resolution, within the same session of analysis (switching automatically the collimator). In Figure 6, an example of this study applied to ELS020 sample is presented. The size of the mapped area was 36 x 13.4 mm (1803 x 671 pixel). For the acquisition of each spectrum in each pixel 50 ms and 4 cycles were used. The red spots represent the accumulation of Ca, which is most probably calcite and contributes to increment the RSD of Ca, whereas the green denser spots, indicating Fe, are usually linked to hematite inclusions. These two type of inclusions are among those more common in the archaeological ceramics.

4.6. The influence of high Pb concentration of Archaeological Ceramics

The Pb is present in two aspects of the archaeological ceramics: in the clay bodies and more significantly in the glazes (of which it is often the main component). If the diffusion front from the glaze into the clay body is very advanced, the concentration of Pb can increase significantly in the proximity of the glaze [46].

The values of Pb registered in the present experiment show a very irregular distribution among the different samples with ranges from $1x10^3$ to $3x10^5$ net counts and presenting RSDs of up to 200%, far beyond the highest RSD showed by the other elements (see Figure 5).

Moreover, an outlying value of $2x10^6$ has been detected for ELS049. With exception of this sample, the Pb concentrations obtained by ICP-MS are in accordance with ED-XRF results, both depicting ELS038 as the Pb richest sample ($12.9\ x10^3$ μg/g). In contrast, ELS049 did not show especially high Pb concentration by ICP-MS ($11.4x10^3$ μg/g). Thus, although the analysis near the glaze was avoided as much as possible, the only explanation for this high value should be the proximity of the lead glaze in the analyses.

As for ED-XRF, the presence of Pb in the ceramic matrices should be critically addressed, since it interferes with the signals of Y, Ga, and Rb, limiting possible discriminating elements [56]. This influence is probably the reason for the decrement on ELS049 and overall high RSD ca. 20-60% showed by both Ga and

Y (see Figure 5). Moreover, they showed concentration values very close to their LOD, thus these elements were not valid for the statistical analysis. In contrast, Rb shows in general lower RSDs (< 25 %) depicting a lower interference on Pb and better concentration ranges (above LOD). However, the net counts show that the highest Pb signal on ELS049 is linked to the lowest Rb value (see Supplementary Material). Although this is not linear, due to the possible interference of Pb, the Rb values should be treated critically in the statistical analysis, especially in Pb rich clay pastes like those presented in this work.

4.7. Clustering by ED-XRF

After measuring all the ceramics the following 24 elements were detected: Mg, Al, Si, P, S, K, Ca, Ti, V, Cr, Mn, Fe, Co, Ni, Cu, Zn, Ga, As, Rb, Sr, Y, Zr, and Pb. In all the cases Kα line of each element was considered, except for Pb where the Lα line was used. Nevertheless, many of the detected elements were not valid for the statistical approach according to these reasons: (i) the proper detection by ED-XRF was not possible as a consequence of the combined effect of the low concentration/small number of counts, (ii) the concentrations of archaeological ceramics were under the LOD or LOQ, (iii) the RSDs observed were too high to be representative and (iv) the signals were influenced by high Pb.

Taking into account the limitations mentioned above, the following elements were considered usable for the statistical treatment: Al, Si, Ca, Ti, Fe, Zr, K and Sr. They were present in the archaeological ceramics in the concentration ranges adequate for their elemental analysis and presented acceptable RSD thresholds.

Nevertheless, the most accurate classification was obtained when omitting Ca and Sr from the statistical analyses (see Figure 3). Apart from the restrictions discussed before for these elements, in the present analytical situation the limited number of discriminant elements biased the classification, giving priority to these major elements and creating clusters which rely more heavily on their concentration. Thus, considering Ca and Sr in the statistical analysis, LOG033 and LOG038 were erroneously associated with TBC groupings. At the same time, TBC was split into three new clusters making the three Basque provenances (ELS, ORD and DUR) indistinguishable. In contrast, the LOG group was better defined since one of its highlights is its lower Ca concentration.

Therefore, a significant improvement was obtained by removing Ca and Sr from the statistical analysis. In spite of their removal, note that the current methodology is not capable of correcting the potential influence of these elements on signals of other elements. This could be another biasing source that should be taken into account, especially in ceramics showing Ca rich pastes.

Figure 3 shows the HCA and PCA using the 6 usable variables obtained by ED-XRF. The mean values for every 50 observations have been used for the HCA analyses, whereas all the observations have been included in the PCA (50 observations per sample). In this way the distribution of the points corresponding to each sample can also be assessed. In the dendrogram obtained by ED-XRF the main separation between TBC and LR is successfully reproduced. Moreover, TBC is split into three further groups, although their hierarchy is now different, showing more isolation for the ORD group instead of DUR. According to the PCA, ORD is dragged down by a higher contribution of Si. In addition, in both cases, LOG038 and LOG033 appear as outliers from the LOG group, although the distances have also changed. The only sample that appears erroneously classified is ELS038, which is the richest in Pb and it appears clustered with DUR.

It should be highlighted that K is a key element to obtain the classification. Frequently, avoiding this element is preferred since it can be altered when analcime is present (see ICP-MS discussion). Although in this case no analcime was reported, the present methodology shows a limitation for analcime bearing ceramics. For instance, the DUR group is separated by both Mn and Mg as seen by ICP-MS, but these could not be used in ED-XRF. Thus, the use of K was compulsory for the proper identification of this group. In contrast, the different values registered for K led to two sub-groupings in LOG samples (not seen by ICP-MS), which can be appreciated by both HCA and PCA obtained by ED-XRF (see Figure 3).

From Figure 3, it can be said that there is a high level of correspondence between the destructively and non-destructively obtained classifications. In any case, the high concentrations of Pb influence the final results. The high Pb values observed for ELS049 were, however, not biasing the classification of this sample within ELS group.

5. Discussion and Conclusions

In this work non-destructive ED-XRF data were subjected to commonly used multivariate statistical methods as a way of evaluating the ability of the non-destructive technique to discriminate among different compositional groups identified after ICP-MS destructive analysis.

The non-destructive multi-point strategy acquiring single-point measurements at 1 mm lateral resolution, (50 replicate analysis per sample), has highlighted the potential of ED-XRF routines for discrimination purposes on medieval and post-Medieval ceramics. These ceramic typologies are characterized by highly decanted ceramic pastes (calcareous and non-calcareous) and the size of their inclusions are rarely higher than 1 mm (see Figure 4). In any case, the clay body should present a minimally homogeneous paste, so that it can be subjected to the present methodology. Therefore, not all matrices would be suitable; like for instance, highly tempered ceramics, such as the well-known cooking pots from Zamora [57], or very roughly decanted pastes, such as those from early stages of ceramic production.

Attending to the concentration ranges and heterogeneity showed by each element, from the concentrations obtained by ED-XRF the following variables could be used for the statistical analysis: Al, Si, K, Ti, Fe, Zr, Ca and Sr. Although the last two were not included as is explained below. Moreover, many elements, fall below the LOD, which is still one of the main limitations to overcome in ED-XRF.

Interestingly, the results provided a positive match between the non-destructively obtained classification, revealing that it can sufficiently approximate the geochemistry of the ceramic paste constituents. Nonetheless, the groups obtained were more defined with the information of ICP-MS analyses. The distances of the dendrogram can serve to illustrate these differences, being up to 3 in the destructive methodology and up to 0.6 in the non-destructive one (see Figure 3). Therefore, the methodology presented in this work could successfully be employed for screening purposes.

Ca and Sr could not be used since when the technological choices (e.g. use of calcareous pastes) are notorious among the dataset, the classification can be biased if these major elements are used, which is due to the insufficient discriminant elements that ED-XRF can provide, whereas by ICP-MS, the large collection of trace and minor elements contribute robustly, in a way that even considering these elements in the statistical analysis the classification remains equal. Moreover, K that can be altered if analcime is present had to be used so that the classification could be obtained, due again to the insufficient discriminant elements. Therefore, the present method might not be valid when analcime driven alterations are relevant.

The main advantage of this methodology is the non-destructive nature of the analysis. Although the cutting of the ceramics involves invasiveness of the technique, this step is crucial in order to prevent post-depositional contaminations and to extract data from the original ceramic matrix. However, this step includes a very low-level of invasiveness compared with the powdering of the samples since the cut fragments can be re-used to perform additional analyses or to be saved.

Moreover, the current methodology requires cheaper and more accessible installation compared with the equipment necessary to carry out ICP-MS analysis, including those used for the sample preparation (fluxer, chemical products, etc.) and the clean room necessary for the analyzer machine.

Further advantages involve the automation possibilities that the set-up used provides, which, thanks to the auto-focus option, allows for the uninterrupted analysis of large batches of samples (both punctual and mapping analysis options). This analysis can be used as a preliminary approach to the archaeological ceramic materials, which thereafter can be selectively subjected to destructive analysis. In this way, not only resources such as money and time are saved, but also the ceramic materials which are irreplaceable remain practically untouched.

The non-destructive methodology presented here provides a preliminary approach for the analysis of archaeological ceramics in determined contexts. With the current setup, this analysis can only be used as a preliminary classification model, whereas the provenance investigations that tend to rely heavily on the concentrations of the minor and trace elements require further refinement of the technique.

Conflicts of interest

There are no conflicts to declare.

Acknowledgments

This research project has been carried out in the framework of the ongoing research funded by the Spanish Ministry of Economy and Competitiveness with the scholarship (BES-2014-068940). Javier G. Iñañez thanks the Spanish Ministry of Economy and Competitiveness for a Ramon y Cajal contract (RYC-2014-16835). The ongoing investigation in which this work is framed receives funding by the projects from the Spanish Ministry of Economy and Competitiveness CERANOR (HAR-2013-46853) and CERANOR-2 (HAR2017-84219-P). The authors would like to acknowledge all the parts involved in this project, with special thanks to those who provided the ceramic pieces; to the Department of Culture of the Basque Government for granting us access to the archaeological material used in this study. The specimens of Orduña were provided by the Archaeological Museum of Biscay (Sonia Cajigas) and those from Elosu, by the Basque Pottery Museum of Ollerias (Blanca Gomez), whereas the specimens from Logroño were kindly provided by ArqueoRioja archaeological company (Teresa Angulo and Fernando Porres).

References

[1] M. D. Glascock, Compositional Analysis in Archaeology, in: Oxford Handbooks, Oxford Handbooks Online, 2016, pp. 1–25. doi:10.1093/oxfordhb/9780199935413.013.8.

[2] S. Gomez Ferrer, J. Buxeda i Garrigós, J. G. Iñañez, F. Amores Carredano, A. Alzate Gallego, Sevillian transport jars in early colonial America: the case of Santa María La Antigua del Darién (Colombia), Open Journal of Archaeometry 1 (1) (2013) 10–15. doi:10.4081/arc.2013.e3.

[3] J. P. Blomster, H. Neff, M. D. Glascock, Olmec pottery production and export in ancient Mexico determined through elemental analysis, Science 307 (5712) (2005) 1068–1072. doi:10.1126/science.1107599.

[4] Weigand, G. Harbottle, E. Sayre, Turquoise sources and source analysis: Mesoamerica and the southwestern USA — University College London, Exchange Systems in Prehistory (1977) 15–34doi:10.1016/B978-0-12-227650-7.50008-0.

[5] J. Buxeda i Garrigós, M. Madrid i Madrid, Designing Rigorous Research: Integrating Science and Archaeology, in: The Oxford Handbook of Archaeological Ceramics, oxford han Edition, Oxford University Press, Oxford, 2017, Ch. Part II. R, pp. 19–47. doi:10.1093/oxfordhb/9780199681532.013.3.

[6] S. C. Phillips, R. J. Speakman, Initial source evaluation of archaeological obsidian from the Kuril Islands of the Russian Far East using portable XRF, Journal of Archaeological Science 36 (6) (2009) 1256–1263. doi:10.1016/j.jas.2009.01.014.

[7] J. G. Iñañez, R. J. Speakman, J. Buxeda i Garrigós, M. D. Glascock, Chemical characterization of tin-lead glazed pottery from the Iberian Peninsula and the Canary Islands: Initial steps toward a better understanding of Spanish Colonial pottery in the Americas, Archaeometry 51 (4) (2009) 546–567. doi:10.1111/j.1475-4754.2008.00431.x.

[8] A. Hein, V. Kilikoglou, Compositional variability of archaeological ceramics in the eastern Mediterranean and implications for the design of provenance studies, Journal of Archaeological Science: Reportsdoi:10.1016/j.jasrep.2017.03.020.

[9] A. M. Pollard, Analytical Chemistry in Archaeology, Cambridge University Press, 2007.

[10] A. M. W. Hunt, The Oxford handbook of archaeological ceramic analysis, 2016.

[11] M. T. Boulanger, S. S. Fehrenbach, M. D. Glascock, Experimental evaluation of sample-extraction methods and the potential for contamination in ceramic specimens, Archaeometry 55 (5) (2013) 880–892. doi:10.1111/j.1475-4754.2012.00706.x.

[12] S. G. D. Madinabeitia, M. S. Lorda, J. G. Ibarguchi, Simultaneous determination of major to ultratrace elements in geological samples by fusion-dissolution and inductively coupled plasma mass spectrometry techniques, Analytica Chimica Acta 625 (2) (2008) 117–130. doi:10.1016/j.aca.2008.07.024.

[13] A. M. W. Hunt, R. J. Speakman, Portable XRF analysis of archaeological sediments and ceramics, Journal of Archaeological Science 53 (2015) 626–638. doi:10.1016/j.jas.2014.11.031.

[14] J. K. Millhauser, E. Rodríguez-Alegría, M. D. Glascock, Testing the accuracy of portable X-ray fluorescence to study Aztec and Colonial obsidian supply at Xaltocan, Mexico, Journal of Archaeological Science 38 (11) (2011) 3141–3152. doi:10.1016/j.jas.2011.07.018.

[15] R. J. Speakman, M. Steven Shackley, Silo science and portable XRF in archaeology: a response to Frahm, Journal of Archaeological Science 40 (2) (2013) 1435–1443. doi:10.1016/j.jas.2012.09.033.

[16] R. D. Kuhn, M. L. Sempowski, A new approach to dating the League of the Iroquois, American Antiquity 66 (2) (2001) 301–314. doi:10.2307/2694610.

[17] R. Fernández-Ruiz, M. García-Heras, Study of archaeological ceramics by total-reflection X-ray fluorescence spectrometry: Semi-quantitative approach, Spectrochimica Acta - Part B Atomic Spectroscopydoi:10.1016/j.sab.2007.06.015.

[18] M. García-Heras, M. J. Blackman, R. Fernández-Ruiz, R. L. Bishop, Assessing Ceramic Compositional Data: A Comparison of Total Reflection X-ray Fluorescence and Instrumental Neutron Activation Analysis On Late Iron Age Spanish Celtiberian Ceramics, Archaeometry 43 (3) (2001) 325–347. doi:10.1111/1475-4754.00020.

[19] C. García-Florentino, M. Maguregui, E. Marguí, L. Torrent, I. Queralt, J. M. Madariaga, Development of Total Reflection X-ray fluorescence spectrometry quantitative methodologies for elemental characterization of building materials and their degradation products, Spectrochimica Acta - Part B Atomic Spectroscopy 143 (2018) 18–25. doi:10.1016/j.sab.2018.02.008.

[20] F. Cariati, P. Fermo, S. Gilardoni, A. Galli, M. Milazzo, A new approach for archaeological ceramics analysis using total reflection X-ray fluorescence spectrometry, Spectrochimica Acta - Part B Atomic Spectroscopy 58 (2) (2003) 177–184. doi:10.1016/S0584-8547(02)00253-7.

[21] A. Ignazio, C. Biancamaria, L. Veronica, T. Roberto, A fast new method for the chemical analysis of clays by Total Reflection X-Ray Fluorescence Spectroscopy (TXRF), in: P. of Bari (Ed.), 3rd International Conference on applied Mineralogy and Advanced Materials, Scientic Research Abstracts, Bari, 2018, p. 2. doi:ISSN:2464-9147.

[22] C. Vanhoof, J. R. Bacon, A. T. Ellis, L. Vincze, P. Wobrauschek, 2018 atomic spectrometry update a review of advances in X-ray fluorescence spectrometry and its special applications, Journal of Analytical Atomic Spectrometry (2018) 1413–1431doi:10.1039/C8JA90030B.

[23] J. Buxeda i Garrigós, Alteration and Contamination of Archaeological Ceramics: The Perturbation Problem, Journal of Archaeological Science 26 (3) (1999) 295–313. doi:10.1006/jasc.1998.0390.

[24] C. Puig, Barrachina, Les produccions ceramiques del Pais Basc durant l'epoca baixmedieval i moderna. Una aproximacio arqueometrica, Ph.D. thesis, Universitat de Barcelona (2016).

[25] F. De Vleeschouwer, V. Renson, P. Claeys, K. Nys, R. Bindler, Quantitative WD-XRF calibration for small ceramic samples and their source material, Geoarchaeology 26 (3) (2011) 440–450. doi:10.1002/gea.20353.

[26] R. J. Speakman, N. C. Little, D. Creel, M. R. Miller, J. G. Iñañez, Sourcing ceramics with portable XRF spectrometers? A comparison with INAA using Mimbres pottery from the American Southwest, Journal of Archaeological Science 38 (12) (2011) 3483–3496. doi:10.1016/j.jas.2011.08.011.

[27] T. Ohmori, M. Hatayama, T. Ohchi, H. Ito, H. Takenaka, K. Tsuji, Development of x-ray 2d dispersive device for wd-xrf imaging spectrometer, Powder Diffraction 27 (2) (2012) 71–74.

[28] S. Palumbo, M. Golitko, S. Christensen, G. Tietzer, Basalt source characterization in the highlands of western panama using portable X-ray fluorescence (pXRF) analysis, Journal of Archaeological Science: Reports 2 (2015) 61–68. doi:10.1016/j.jasrep.2015.01.006.

[29] P. J. Sheppard, G. J. Irwin, S. C. Lin, C. P. McCaffrey, Characterization of New Zealand obsidian using PXRF, Journal of Archaeological Science 38 (1) (2011) 45–56. doi:10.1016/j.jas.2010.08.007.

[30] C. García-Florentino, M. Maguregui, H. Morillas, I. Marcaida, J. M. Madariaga, A fast in situ non-invasive approach to classify mortars from a construction of high historical value, Microchemical Journal 133 (2017) 104–113. doi:10.1016/j.microc.2017.03.020.

[31] N. Forster, P. Grave, N. Vickery, L. Kealhofer, Non-destructive analysis using PXRF: methodology and application to archaeological ceramics, X-Ray Spectrometry 40 (5) (2011) 389–398. doi:10.1002/xrs.1360.

[32] M. M. Martínez González, La producción cerámica en la Baja Edad Media: el alfar de la calle Hospital Viejo de Logroño (La Rioja), Ph.D. thesis, Universidad de la Rioja (2013).

[33] E. Calparsoro, G. Arana, J. Iñañez, Pottery from orduña village in the 17th–19th centuries: an archaeometrical approach, Journal of Archaeological Science: Reports 23 (2019) 304–323.

[34] A. Rodríguez Miranda, J. Valle Melón, E. Calparsoro, J. G. Iñañez, Study, revalorization and virtual musealization of a ceramic kiln based on information gathered from old excavations, Digital Applications in Archaeology and Cultural Heritage 7. doi:10.1016/j.daach.2017.08.003.

[35] Enrike Ibabe Ortiz, Ceramica popular vasca, Bilbao Bizkaia Kutxa, 1995.

[36] E. Calparsoro, M. Glascock, T. Angulo, F. Porres, J. Ceniceros, J. G. Iñañez, An Archaeometric Approach to Pottery from the Basque Country and La Rioja (13th-18th) by Means of NAA (2016).

[37] J. Aitchison, The Statistical Analysis of Compositional Data, Journal of the Royal Statistical Society. Series B. Methodological 44 (2) (1982) 139–177. doi:10.2307/2345821.

[38] J. Buxeda i Garrigós, V. Kilikoglou, Total Variation as a Measure of Variability in Chemical Data Sets, in: L. van Zelst (Ed.), Patterns and Process. A Festchrift in honor to Dr. Edward Sayre, Smithsonian Center forMaterials Research and Education, Suitland, Maryland, 2003, pp. 185–198.

[39] R. L. Bishop, H. Neff, Compositional data analysis in archaeology., in: Archaeological chemistry IV, 1989, pp. 57–86. doi:doi:10.1021/ba-1988-0220.ch004.

[40] S. Shennan, Quantifying archaeology, Edinburgh University Press, 1988.

[41] D. Sayre, E.V., Harbottle, G., Bieber, A.M., Brooks, Application of Multivariative Techniques to Analytical Data on Aegean Ceramics, Archaeometry 18 (1) (1976) 59–74. doi:10.1111/j.1475-4754.1976.tb00145.x.

[42] H. Neff, Neutron activation analysis for provenance determination in archaeology, in: Modern Analytical Methods in Art and Archaeology, 2000.

[43] J. Aitchison, The Statistical Analysis of Compositional Data, Monographs on Statistics and Applied Probability.

[44] K. G. van den Boogaart, R. Tolosana, M. Bren, Compositions: compositional data analysis, R package version (2010) 1–10.

[45] GitHub Online Repository of ArchFlow. www.github.com/esteful/arch_flow [online] (2018).

[46] J. Molera, T. Pradell, N. Salvado, Interactions between clay bodies and lead glazes, Journal of the American Ceramic Society 84 (5) (2001) 1120–1128. doi:10.1111/j.1151-2916.2001.tb00799.x.

[47] I. Freestone, Retention of Phosphate in Buried Ceramics: An electron microbeam approach, Archaeomtery 27 (2).

[48] J. Buxeda i Garrigós, H. Mommsen, A. Tsolakidou, Alterations of Na, K and Rb concentrations in Mycenaean pottery and a proposed explanation using X-ray diffraction, Archaeometry 44 (2) (2002) 187–198. doi:10.1111/1475-4754.t01-1-00052.

[49] A. Schwedt, H. Mommsen, N. Zacharias, J. Buxeda i Garrigós, Analcime crystallization and compositional profiles - Comparing approaches to detect post-depositional alterations in archaeological pottery, Archaeometry 48 (2) (2006) 237–251. doi:10.1111/j.1475-4754.2006.00254.x.

[50] B. Fabbri, S. Gualtieri, S. Shoval, The presence of calcite in archeological ceramics, Journal of the European Ceramic

Society 34 (7) (2014) 1899–1911.

[51] E. Calparsoro, G. Arana, T. Angulo, F. Porres, J. G. Iñañez, An archaeometrical approach to the pottery from Hospital Viejo street in Logroño (La Rioja, Spain), ArcheoSciences.

[52] J. Pérez-Arantegui, M. Resano, E. García-Ruiz, F. Vanhaecke, C. Roldán, J. Ferrero, J. Coll, Characterization of cobalt pigments found in traditional Valencian ceramics by means of laser ablation-inductively coupled plasma mass spectrometry and portable X-ray fluorescence spectrometry, Talanta 74 (5) (2008) 1271–1280. doi:10.1016/j.talanta.2007.08.044.

[53] L. H. Keith, W. Crummett, J. Deegan, R. A. Libby, J. K. Taylor, G. Wentler, Principles of environmental analysis, Analytical chemistry 55 (14) (1983) 2210–2218.

[54] B. Beckhoff, B. Kanngie_er, N. Langhoff, R. Wedell, H. Wolff, Handbook of Practical X-Ray Fluorescence Analysis, 2007.

[55] E. Frahm, Validity of off-the-shelf handheld portable XRF for sourcing Near Eastern obsidian chip debris, Journal of Archaeological Science 40 (2) (2013) 1080–1092. doi:10.1016/j.jas.2012.06.038.

[56] N. Forster, P. Grave, Effects of elevated levels of lead in ceramics on provenancing studies using non-destructive PXRF: A case study in byzantine cypriot glazed ceramics, X-Ray Spectrometry 42 (6) (2013) 480–486. doi:10.1002/xrs.2507.

[57] U. Sanchez-garmendia, C. Estefania, G. Arana, J. G. Iñañez, Beneath sacred land : glazed pottery from the old Church of La Concepción in Zamora, in: Glaze Art Lisbon, Lisbon, 2018.

Figure 1: Sample description showing their photographs, chronologies and locations.

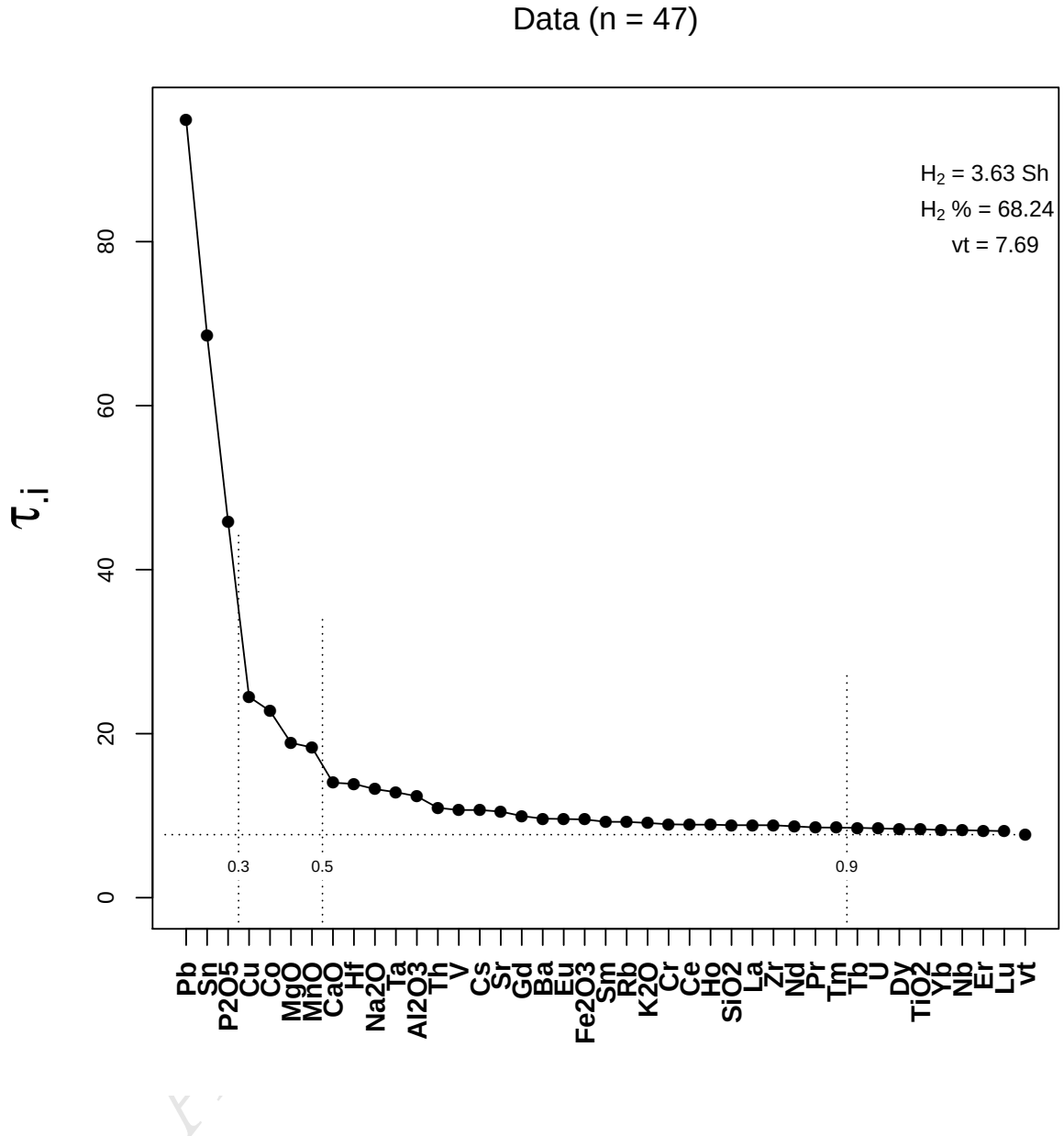

Figure 2: Graphical representation of the compositional variation matrix for 47 samples based concentrations obtained by ICP-MS. ν_τ = Total variation, H_2 = information entropy, $H_2\%$ = percentage of information entropy over the maximum possible, n = number of specimens

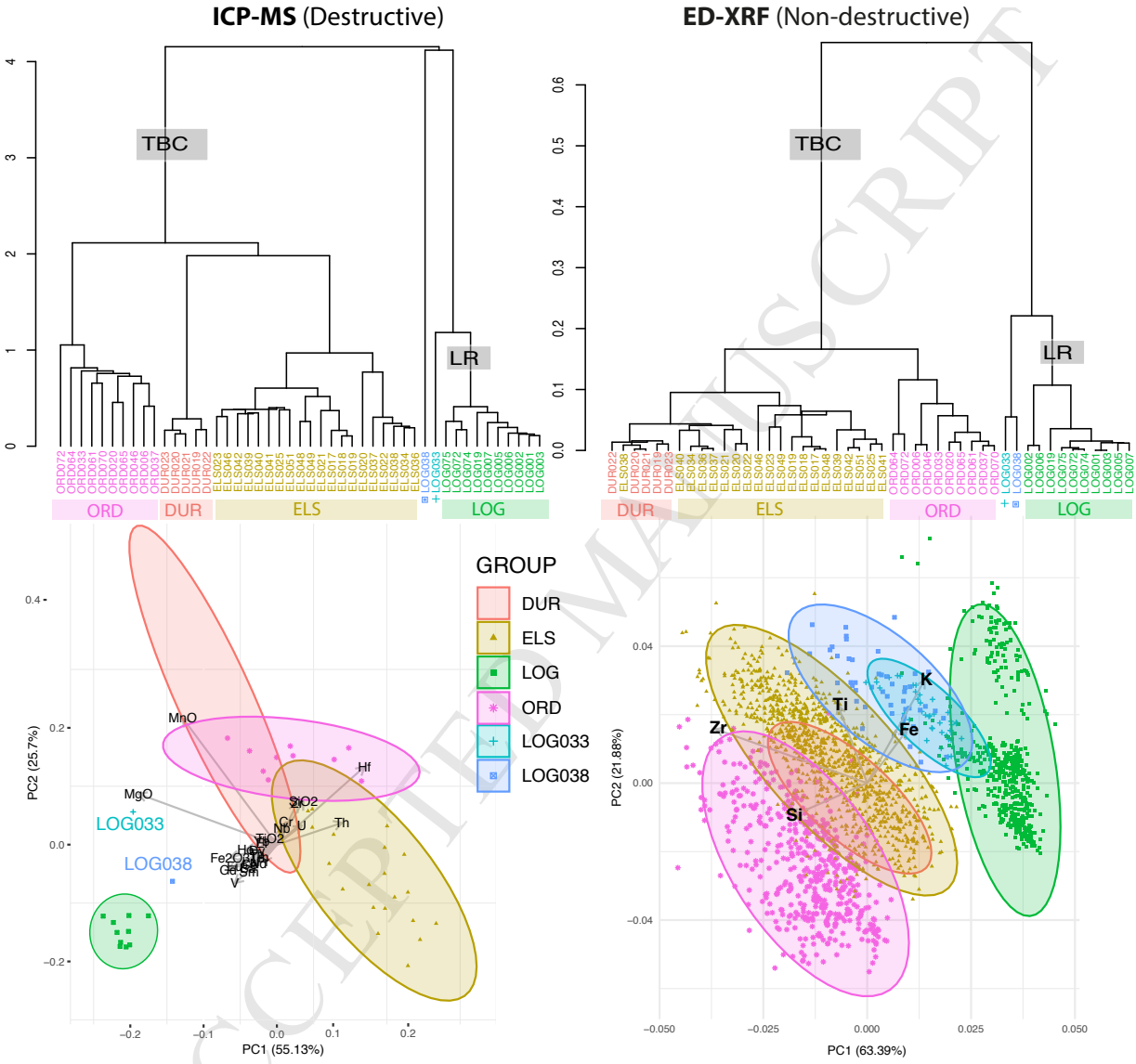

Figure 3: HCA and PCA of the data obtained by ICP-MS (left) and ED-XRF (right). The clr and alr transformed values are used for HCA and PCA respectively, including the following elements in the case of ICP-MS: MgO, Al_2O_3, SiO_2, TiO_2, Fe_2O_3, MnO, V, Cr, Zr, Nb, Ba, Hf, La, Ce, Pr, Nd, Sm, Eu, Gd, Tb, Dy, Ho, Er, Er, Tm, Yb, Th and U and, in the case of ED-XRF: Si, Ti, Fe, Zr and K. In the PCAs Lu and Al have been used as divisors for ICP-MS and ED-XRF, respectively. Ellipses represent a confidence interval of 95%.

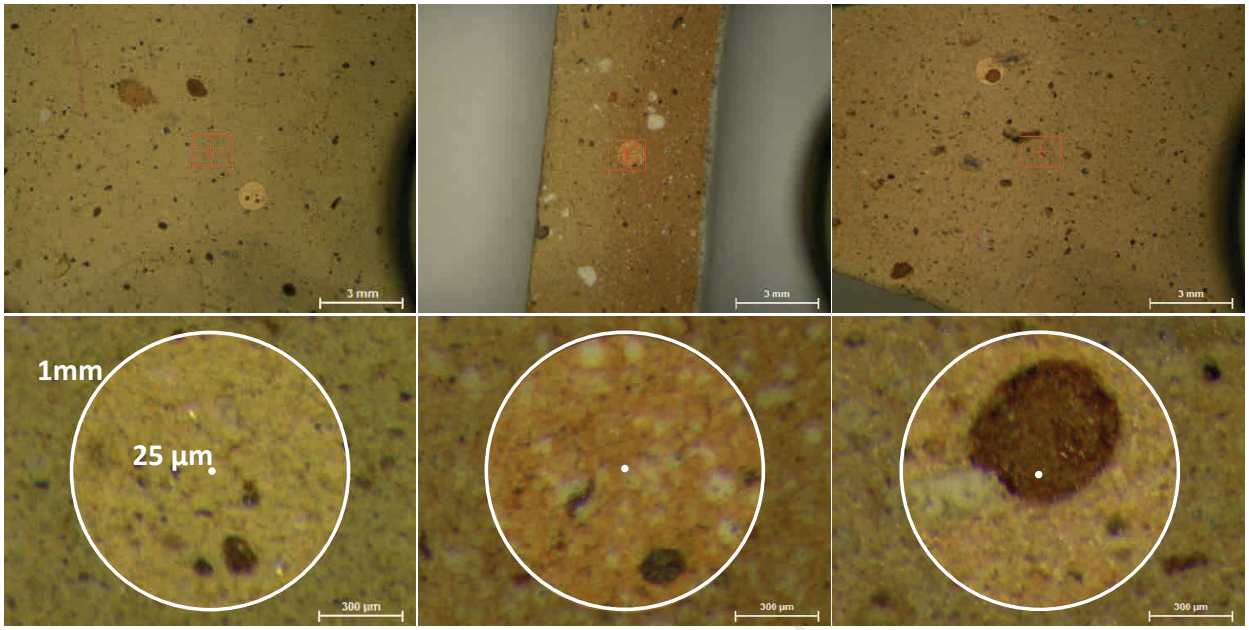

Figure 4: Different ceramic samples showing the pastes' heterogeneity level and the spot size obtained with both lateral resolutions: 25 μm and 1 mm.

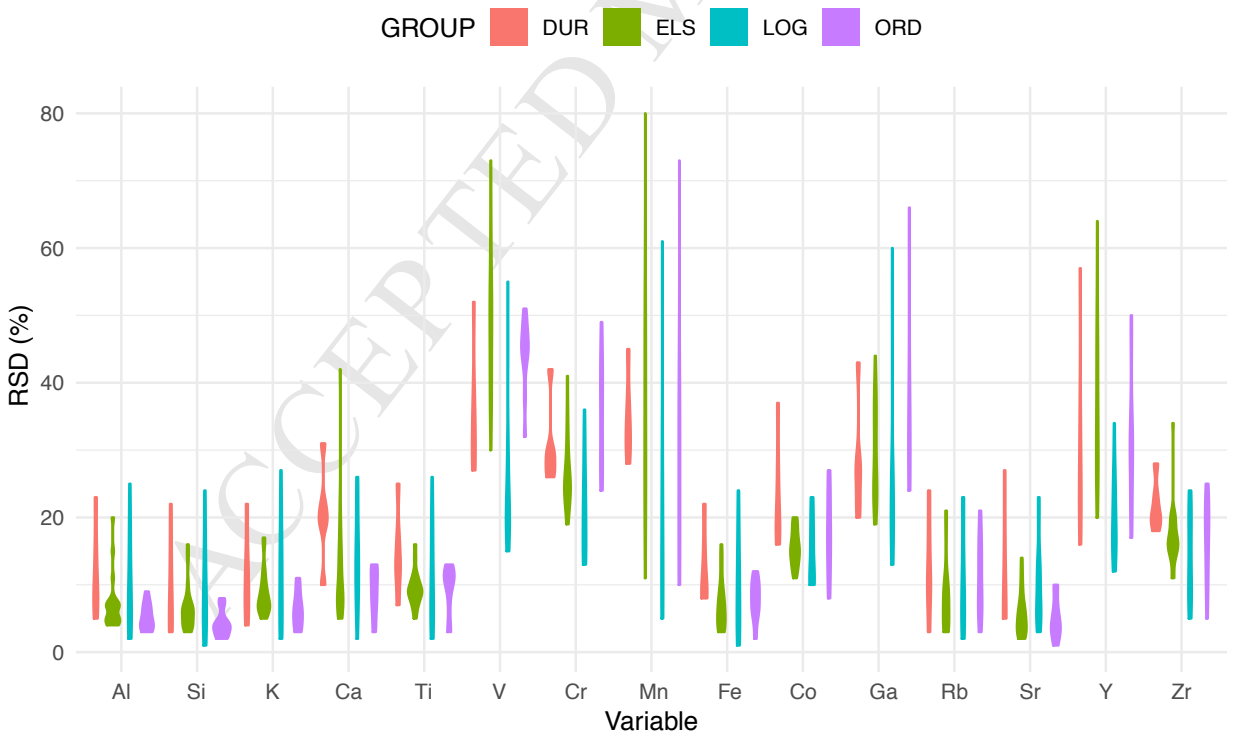

Figure 5: Violin plot showing RSD (%) values, from 50 replicate analysis corresponding to each group. Pb presented over 200% RSD and is not included in the chart. Note that not all elements were above LOQ and/or LOQ.

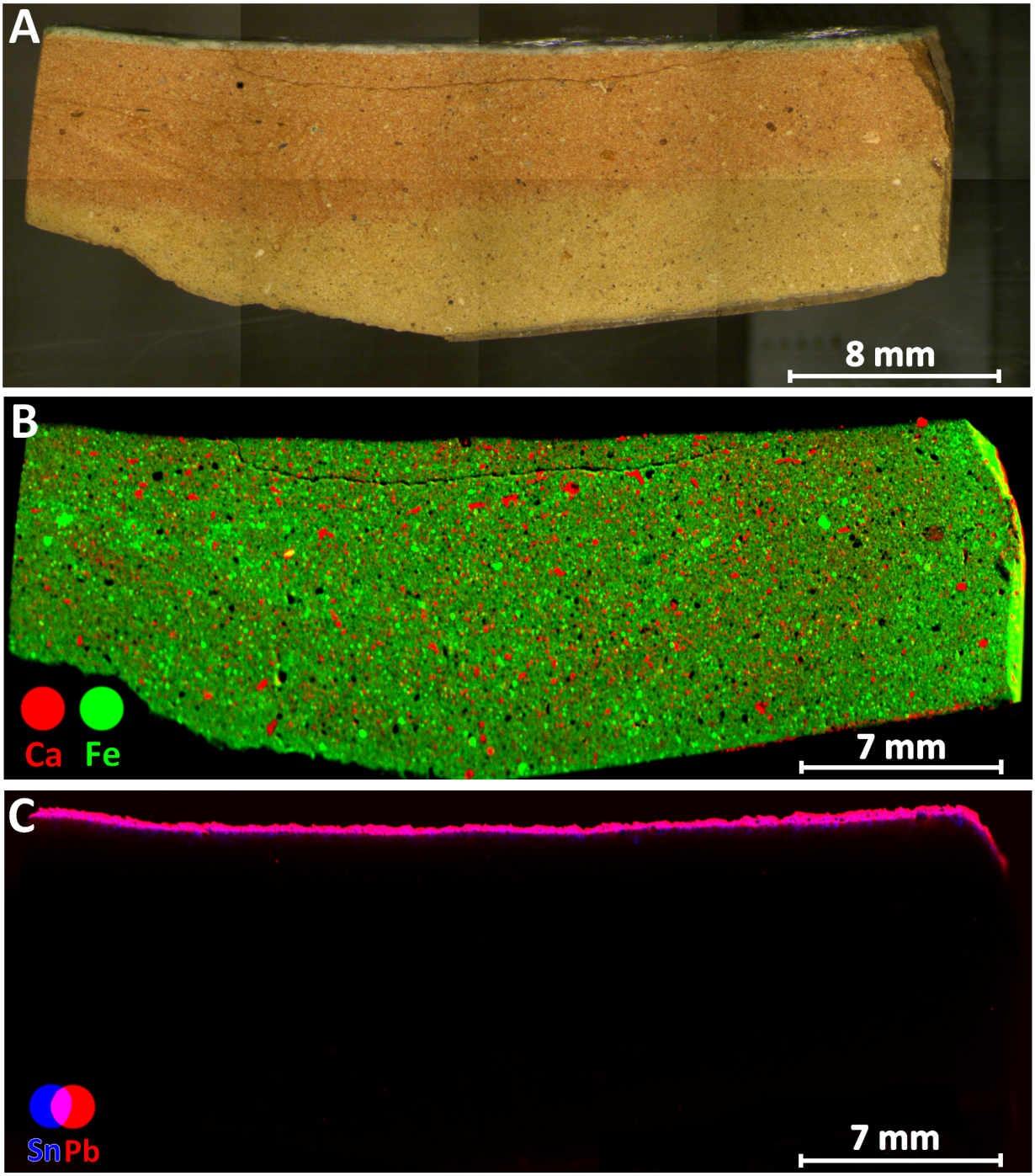

Figure 6: Image of the sample ELS020 (A) and elemental Mapping obtained by ED-XRF at down to 25μm, showing Ca and Fe major elements distributions (B) and Sn and Pb glaze related elements (C).